OX40L blockade protects against inflammation-driven fibrosis

Muriel Elhai[a,b,1], Jérôme Avouac[a,b,1], Anna Maria Hoffmann-Vold[c], Nadira Ruzehaji[a], Olivia Amiar[a], Barbara Ruiz[a], Hassina Brahiti[a], Matthieu Ponsoye[a], Maxime Fréchet[a], Anne Burgevin[a], Sonia Pezet[a], Jérémy Sadoine[d,e], Thomas Guilbert[a], Carole Nicco[a], Hisaya Akiba[f], Vigo Heissmeyer[g,h], Arun Subramaniam[i], Robert Resnick[i], Øyvind Molberg[c], André Kahan[b], Gilles Chiocchia[j], and Yannick Allanore[a,b,2]

[a]INSERM, U1016 UMR8104, Cochin Institute, Paris Descartes University, Sorbonne Paris Cite, 75014 Paris, France; [b]Rheumatology A Department, Cochin Hospital, Paris Descartes University, 75014 Paris, France; [c]Department of Rheumatology, Oslo University Hospital, 0873 Oslo, Norway; [d]Equipe d'Accueil (EA) 2496 Pathologie, Imagerie et Biothérapies Orofaciales, Faculty of Odontology, Paris Descartes University, Sorbonne Paris Cite, 92120 Montrouge, France; [e]Plateforme d'Imagerie Du Vivant, Le Pôle de Recherche et d'Enseignement Supérieur Sorbonne Paris Cité, 92120 Montrouge, France; [f]Department of Immunology, Juntendo University School of Medicine, Tokyo 113-8421, Japan; [g]Research Unit Molecular Immune Regulation, Institute of Molecular Immunology, Helmholtz Zentrum München, DE-81377 Munich, Germany; [h]Institute for Immunology, Ludwig-Maximilians-Universität München, DE-80336 Munich, Germany; [i]Immune Mediated Diseases, Sanofi Genzyme, Framingham, MA 01701; and [j]INSERM, U1173, Faculty of Health Sciences Simone Veil, Université Versailles-Saint-Quentin, 78180 Saint-Quentin-En-Yvelines, France

Edited by Marc Feldmann, Kennedy Institute of Rheumatology, Oxford, United Kingdom, and approved April 28, 2016 (received for review November 27, 2015)

Treatment for fibrosis represents a critical unmet need, because fibrosis is the leading cause of death in industrialized countries, and there is no effective therapy to counteract the fibrotic process. The development of fibrosis relates to the interplay between vessel injury, immune cell activation, and fibroblast stimulation, which can occur in various tissues. Immunotherapies have provided a breakthrough in the treatment of immune diseases. The glycoprotein OX40–OX40 ligand (OX40L) axis offers the advantage of a targeted approach to costimulatory signals with limited impact on the whole immune response. Using systemic sclerosis (SSc) as a prototypic disease, we report compelling evidence that blockade of OX40L is a promising strategy for the treatment of inflammation-driven fibrosis. OX40L is overexpressed in the fibrotic skin and serum of patients with SSc, particularly in patients with diffuse cutaneous forms. Soluble OX40L was identified as a promising serum biomarker to predict the worsening of lung and skin fibrosis, highlighting the role of this pathway in fibrosis. In vivo, OX40L blockade prevents inflammation-driven skin, lung, and vessel fibrosis and induces the regression of established dermal fibrosis in different complementary mouse models. OX40L exerts potent profibrotic effects by promoting the infiltration of inflammatory cells into lesional tissues and therefore the release of proinflammatory mediators, thereafter leading to fibroblast activation.

systemic sclerosis | fibrosis | costimulation | OX40L | translational approach

Although they contribute to up to 45% of deaths in the industrialized countries, until now little progress has been made in deciphering fibrotic diseases (1). Nonetheless, it has been demonstrated that pulmonary, renal, hepatic, and even dermal fibrosis share common pathways that drive the pathologic events. In all these tissues, the development of fibrosis relates to the interplay between immune cell activation and fibroblast stimulation, and perpetuation of the fibrotic process leads to progressive impaired organ function. Systemic sclerosis (SSc) is an autoimmune T-cell disease that is defined by pathological fibrosis of the skin and also of internal organs such as lungs (2). Therefore SSc is considered a prototype entity for studying the pathogenesis of fibrosis in fibrotic diseases and particularly the links between inflammation/autoimmunity and fibrosis. Immunotherapies have provided a breakthrough in several autoimmune diseases, such as rheumatoid arthritis, but are associated with increased risk of infections. An emerging therapeutic approach for T-cell–mediated diseases is targeting the antigen-specific T cells involved in the disease without leading to generalized immunosuppression (3). The glycoprotein OX40–OX40 ligand (OX40L) pair, which is involved in late T-cell costimulatory signaling and is transiently expressed following antigen recognition, fits these criteria (4). Blocking OX40–OX40L was effective in preventing the development of disease in several in vivo animal models of autoimmune and inflammatory diseases (5). This strategy has not yet been evaluated in fibrotic conditions such as SSc. Genetic data have shown that *TNFSF4*, which encodes for OX40L, is an SSc susceptibility gene, suggesting a potential role of this pathway in SSc, although the functional effects of the gene variants are not known (6–8). Preliminary results have shown that serum soluble OX40 levels were significantly increased in SSc patients as compared with healthy individuals (9). OX40L blockade was shown to be more effective than OX40 blockade in reducing autoimmunity in the murine model of collagen-induced arthritis, suggesting that signaling via OX40L (and not via OX40) promotes inflammation and autoimmunity (10). Therefore we chose to study the role of OX40L in patients with SSc and in vivo in complementary murine models of SSc. The role of

Significance

Fibrosis is a leading cause of death in industrialized countries. Until now, there has been no effective therapy to prevent or counteract the fibrotic process. This article describes the effect of the blockade of a late costimulatory molecule to prevent inflammation-driven skin, lung, and vessel fibrosis and to induce regression of established dermal fibrosis in vivo in complementary murine models of systemic sclerosis, a prototypic autoimmune fibrotic disease. This article also reveals an unexpected role of this protein as a biomarker of worsening fibrosis that might help delineate the prognosis of patients in clinical practice more accurately.

Author contributions: M.E., J.A., A.K., G.C., and Y.A. designed research; M.E., J.A., A.M.H.-V., N.R., O.A., B.R., H.B., M.P., M.F., A.B., S.P., R.R., and Ø.M. performed research; M.E., J.A., A.M.H.-V., N.R., J.S., T.G., C.N., H.A., V.H., A.S., R.R., Ø.M., and Y.A. contributed new reagents/analytic tools; M.E., J.A., A.M.H.-V., N.R., O.A., B.R., H.B., A.S., R.R., Ø.M., and Y.A. analyzed data; and M.E., J.A., and Y.A. wrote the paper.

Conflict of interest statement: A.S. and R.R. work for Sanofi. J.A. has/had consultancy relationship and/or has received research funding in relationship with the treatment of systemic sclerosis from Actelion, Bayer, BMS, Roche-Chugai, Pfizer, and Sanofi. Y.A. has/had consultancy relationship and/or has received research funding in relationship with the treatment of systemic sclerosis from Actelion, Bayer, Biogen Idec, Bristol-Myers Squibb, Genentech/Roche, Inventiva, Medac, Pfizer, Sanofi/Genzyme, Servier, and Union chimique belge.

This article is a PNAS Direct Submission.

Data deposition: All microarray data and information have been submitted to the National Center for Biotechnology Information Gene Expression Omnibus (accession no. GSE73705).

See Commentary on page 7291.

[1]M.E. and J. A. contributed equally to this work.

[2]To whom correspondence should be addressed. Email: yannick.allanore@cch.aphp.fr.

This article contains supporting information online at www.pnas.org/lookup/suppl/doi:10.1073/pnas.1523512113/-/DCSupplemental.

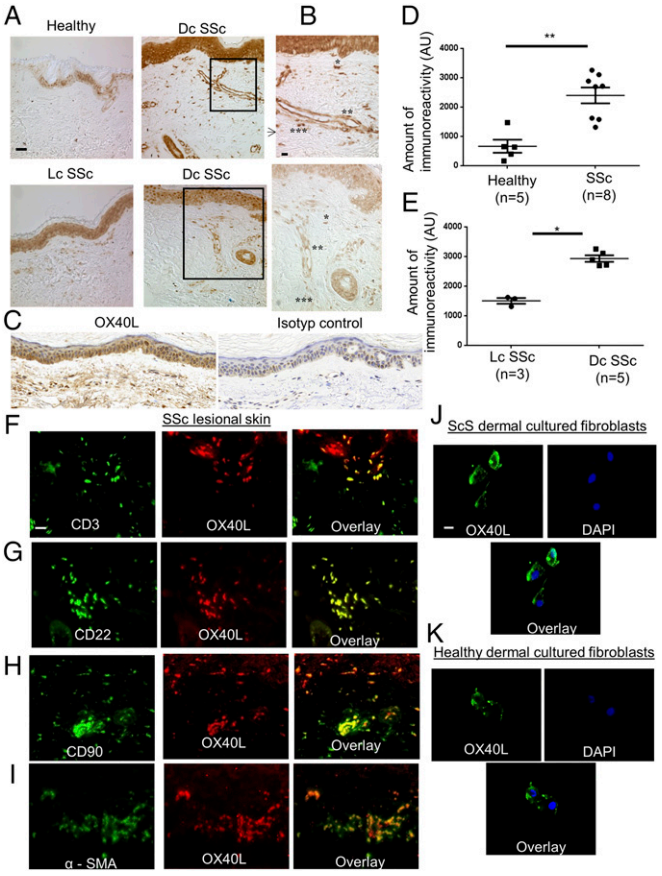

Fig. 1. OX40L is overexpressed by B cells, T cells, and fibroblasts in fibrotic skin of patients with SSc. (*A*) Sections of skin biopsies stained for OX40L were obtained from healthy controls and from the lesional skin of patients with SSc. Four representative tissue sections are shown. (Magnification: 200×.) (Scale bar: 50 μm.) Dc SSc: diffuse cutaneous systemic sclerosis. Lc SSC, limited cutaneous systemic sclerosis. (*B*) Sections of diffuse SSc lesional skin stained for OX40L. (Magnification: 400×.) (Scale bar: 25 μm.) Single asterisks indicate fibroblasts (spindle-shape aspect); double asterisks indicate endothelial cells; triple asterisks indicate inflammatory cells (spherical/ovoid aspect and localized in perivascular area). (*C*) Skin biopsies from a patient with SSc stained for OX40L and for an isotype control. (Magnification: 200×.) (*D* and *E*) Semiquantitative analysis of immunostaining intensity using ImageJ software. Values are represented by dot blots with the mean ± SEM. $*P < 0.05$; $**P < 0.01$; two-tailed Mann–Whitney test. AU: arbitrary units. (*F–I*) Sections of skin biopsies from patients with SSc stained by immunofluorescence for OX40L and CD3 (*F*), CD22 (*G*), CD90 (*H*), and α-SMA (*I*). (Magnification: 400×.) (Scale bar: 10 μm.) (*J* and *K*) Fibroblasts obtained from lesional skin of patients with scleroderma (*J*) and from healthy controls (*K*). Nuclei were stained by DAPI. (Magnification: 630×.) (Scale bar: 5 μm.) The staining was performed in three independent series.

OX40L in SSc was highlighted by the overexpression of the protein in the skin and serum of patients with SSc, particularly in patients with diffuse cutaneous SSc, the most severe and fibrotic form of the disease. Soluble OX40L also was identified as a promising biomarker predictive of fibrosis worsening in patients with SSc. In vivo, blocking OX40L prevented inflammation-driven dermal fibrosis, fibrosing alveolitis, and lung vessel remodeling in complementary murine models of SSc, suggesting that the anti-OX40L antibody offers a promising strategy for the treatment of the inflammatory stages of fibrotic diseases.

Results

OX40L Is Overexpressed in the Skin of Patients with SSc. The expression of OX40L protein was 3.6-fold higher in fibrotic skin of patients with SSc, particularly in patients with diffuse cutaneous forms (Fig. 1 *A–E*), than in the skin of healthy controls ($P = 0.003$). As expected, OX40L was expressed by $CD3^+$ T cells and $CD22^+$ B cells (Fig. 1 *F* and *G*) as well as by endothelial cells (Fig. 1*B*) (4). OX40L staining also was identified in $CD90^+$ and α-smooth muscle actin (α-SMA)-positive cells in SSc skin (Fig. 1 *H* and *I*), suggesting that OX40L is expressed by fibroblasts and myofibroblasts in fibrotic skin. The expression of OX40L by dermal fibroblasts from both patients with SSc and healthy controls was confirmed in vitro (Fig. 1 *J* and *K*).

Soluble OX40L as a Biomarker of Fibrosis. In a cross-sectional analysis soluble OX40 levels were significantly higher in patients with SSc ($n = 177$), particularly in patients with the diffuse cutaneous subset, than in healthy controls ($n = 100$) (Fig. 2*A*). Longitudinal analyses showed that a high OX40L level in serum at baseline was highly predictive of worsening of dermal fibrosis during the follow-up period [hazard ratio (HR): 8.28, 95% confidence interval (CI): 2.11–32.50; $P < 0.001$] (Fig. 2*B*). The association between fibrosing alveolitis and baseline OX40L serum levels was nonsignificant $P = 0.266$ (Fig. S1), but a high OX40L serum level at baseline was highly predictive of pulmonary worsening during the follow-up period (HR: 4.60, 95% CI:1.52–12.18, $P < 0.001$) (Fig. 2*C*).

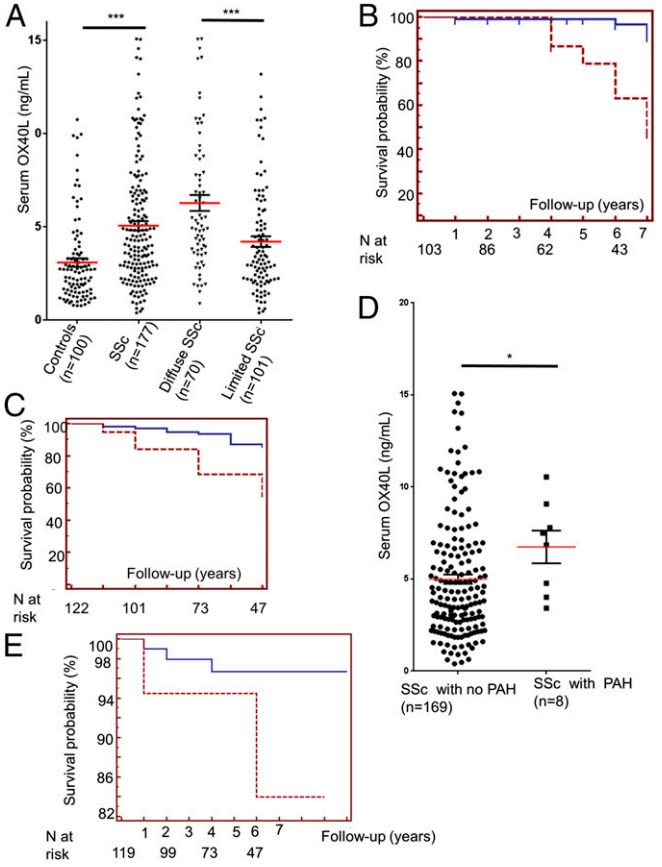

Fig. 2. Soluble OX40L is overexpressed in the serum of patients with SSc and is predictive of worsening of fibrosis. (*A*) Serum OX40L levels in patients with SSc ($n = 177$) and in healthy controls ($n = 100$). (*B*, *C*, and *E*) Kaplan–Meier survival curves for worsening of dermal fibrosis (*B*), lung fibrosis (*C*) and de novo development of PAH (*E*) during the follow-up period according to OX40L levels in serum at baseline. The dashed line represents survival probability in patients with high OX40L levels in serum at baseline (concentration equal to or above the 95th percentile in healthy controls, i.e., 8.4370). The solid line represents survival probability in patients with low OX40L levels in serum at baseline (concentration below the 95th percentile in healthy controls, i.e., 8.4370). The number of patients with SSc at risk is noted below the curves. (*D*) Serum OX40L levels in patients with SSc with ($n = 8$) and without ($n = 169$) PAH. $*P < 0.05$.

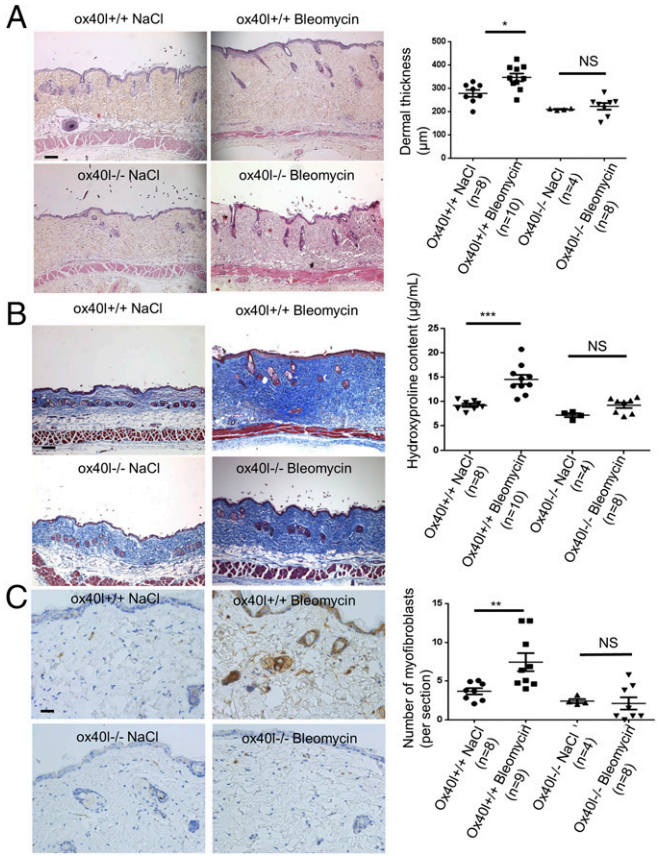

Fig. 3. Mice lacking OX40L are protected from dermal fibrosis induced by bleomycin. (*A*) Representative H&E-stained sections (magnification: 100×) from ox40l$^{+/+}$ mice injected s.c. with NaCl (n = 8), ox40l$^{+/+}$ mice injected s.c. with bleomycin (n = 10), ox40l$^{-/-}$ mice injected s.c. with NaCl (n = 4), and ox40l$^{-/-}$ mice injected s.c. with bleomycin (n = 8). (Scale bar: 100 μm.) (*B*) Representative sections stained by trichrome. (Magnification: 100×.) (Scale bar: 100 μm.) Hydroxyproline content is reduced in lesional skin of ox40l$^{-/-}$ mice. (*C*) Myofibroblasts were identified by positive staining for α-SMA in slides after counterstaining with hemalun. (Scale bar: 50 μm.) Values are represented by dot blots with the mean ± SEM. The experiment was performed in two independent series. *P < 0.05; **P < 0.01; ***P < 0.001; two-sided Mann–Whitney test. NS: nonsignificant.

Patients with SSc and pulmonary arterial hypertension (PAH) had higher OX40L serum levels at baseline (6.74 ± 3.31 ng/mL versus 4.99 ± 3.29; P < 0.05) (Fig. 2*D*). A trend was seen for patients with elevated serum OX40L levels at baseline to develop de novo PAH more frequently than patients with a low OX40L concentration (HR: 3.64, 95% CI: 0.32–41.02; P = 0.13) (Fig. 2*E*), but the small number of patients preclude any firm conclusions.

In the replication cohort (n = 241), OX40L was highly associated with lung fibrosis in the cross-sectional analysis (regression coefficient B: 0.003, SE 0.001, P = 0.025). At follow-up, OX40L was predictive for worsening lung fibrosis both in univariate (P = 0.002) and multivariate linear regression models (HR: 1.5, 95% CI: 1.03–2.31; P = 0.037) (Table S1). These results emphasize the role of OX40L in SSc and in fibrosis and suggest that OX40L might be used as a biomarker to delineate the prognosis of patients with SSc more accurately in clinical practice. To assess the role of OX40L in fibrosis further, the effect of OX40L blockade on fibrosis was evaluated in vivo in different complementary murine models of SSc.

OX40L-Deficient Mice Are Protected from Bleomycin-Induced Dermal Fibrosis. ox40l$^{-/-}$ mice were markedly protected from bleomycin-induced fibrosis with a mean ± SEM decreases of 13 ± 7% in dermal thickness (P = 0.027), 19 ± 8% (P = 0.034) in hydroxyproline content, and 57 ± 32% (P = 0.044) in myofibroblast count in the lesional skin of ox40l$^{-/-}$ mice compared with ox40l$^{+/+}$ mice after bleomycin injections (Fig. 3).

OX40L Invalidation Reduces T Cells, B Cells, Natural Killer Cells, and Macrophage Infiltration in Lesional Skin of Mice Challenged with Bleomycin. CD3$^+$ T cells were reduced by 64 ± 8% (P = 0.029), CD22 B cells were reduced by 71 ± 9% (P = 0.016), natural killer (NK) cells were reduced by 72% ± 26% (P = 0.029), and CD68 macrophages were reduced by 74 ± 3% (P = 0.029) in lesional skin of ox40l$^{-/-}$ mice as compared with ox40l$^{+/+}$ mice treated with bleomycin (Fig. 4 *A*–*D*).

OX40L Invalidation Reduces Levels of Proinflammatory Cytokines in the Lesional Skin of Mice Challenged with Bleomycin. ox40l$^{-/-}$ mice showed reduced levels of IL-6 (56 ± 9%, P = 0.029) and TNF-α (66 ± 2%, P = 0.016) after bleomycin treatment (Fig. 4 *E* and *F*). No differences in the levels of IL-4 and IL-10 were observed, but there was a nonsignificant trend for decreased IL-17 and IFN-γ (Fig. S2).

OX40L Invalidation Induces Gene-Expression Changes in the Lesional Skin of Mice Challenged with Bleomycin. To identify the downstream pathways affected by OX40L inhibition, gene expression was compared in ox40l$^{+/+}$ and ox40l$^{-/-}$ mice injected with bleomycin. Five top key cell functions (Table 1) and five canonical pathways (Table 2) were identified by supervised analysis. Inhibition of matrix metalloproteinase (MMP) was a relevant pathway in the context of fibrosis (P = 0.020). The main genes identified in this pathway were MMP-28, thrombospondin-2, and tissue factor pathway inhibitor-2. Gene set enrichment analysis identified the NF-κB, and activator protein 1 (AP-1) pathways as down-regulated in ox40l$^{-/-}$ mice (Table 3).

OX40L Regulates Inflammatory and Myofibroblast Lesional Skin Infiltration Through AP-1. AP-1 regulates the gene expression of MMP1 and TIMP1, which are involved in matrix remodeling. Furthermore, AP-1 is up-regulated in a TGF-β–dependent manner in SSc, and pharmacological inhibition of AP-1 prevents the pathological activation of dermal fibroblasts in vitro and the development of experimental dermal fibrosis in different in vivo models (11) Therefore we focused on the AP-1 pathway by studying the expression of two well-known AP-1 proteins. c-fos and c-jun, in the lesional skin of mice treated with bleomycin. c-Fos was detected on T cells and myofibroblasts, with fewer myofibroblasts expressing c-fos in the lesional skin of ox40l$^{-/-}$ mice than in ox40l$^{+/+}$ mice (P = 0.0260) (Fig. 4 *G*–*J*). A decrease in the expression of c-jun was also observed in ox40l$^{-/-}$ mice treated with bleomycin (Fig. S3).

OX40L Blockade Prevents Dermal Fibrosis by Acting on both Hematopoietic and Nonhematopoietic Cells. To determine whether OX40L blockade acts predominantly on inflammatory cells or fibroblasts to prevent

Table 1. Ingenuity knowledge base analysis

Molecular and cellular functions	No. of differentially expressed genes	P value
Cellular assembly and organization	28	1.74×10^{-4}
Cellular function and maintenance	20	2.59×10^{-4}
Molecular transport	13	6.60×10^{-4}
Protein trafficking	12	6.60×10^{-4}
Posttranslational modification	13	1.47×10^{-3}

A transcriptomic approach was performed to compare genes differentially expressed between ox40l$^{+/+}$ (n = 3) and ox40l$^{-/-}$ mice (n = 4) injected with bleomycin.

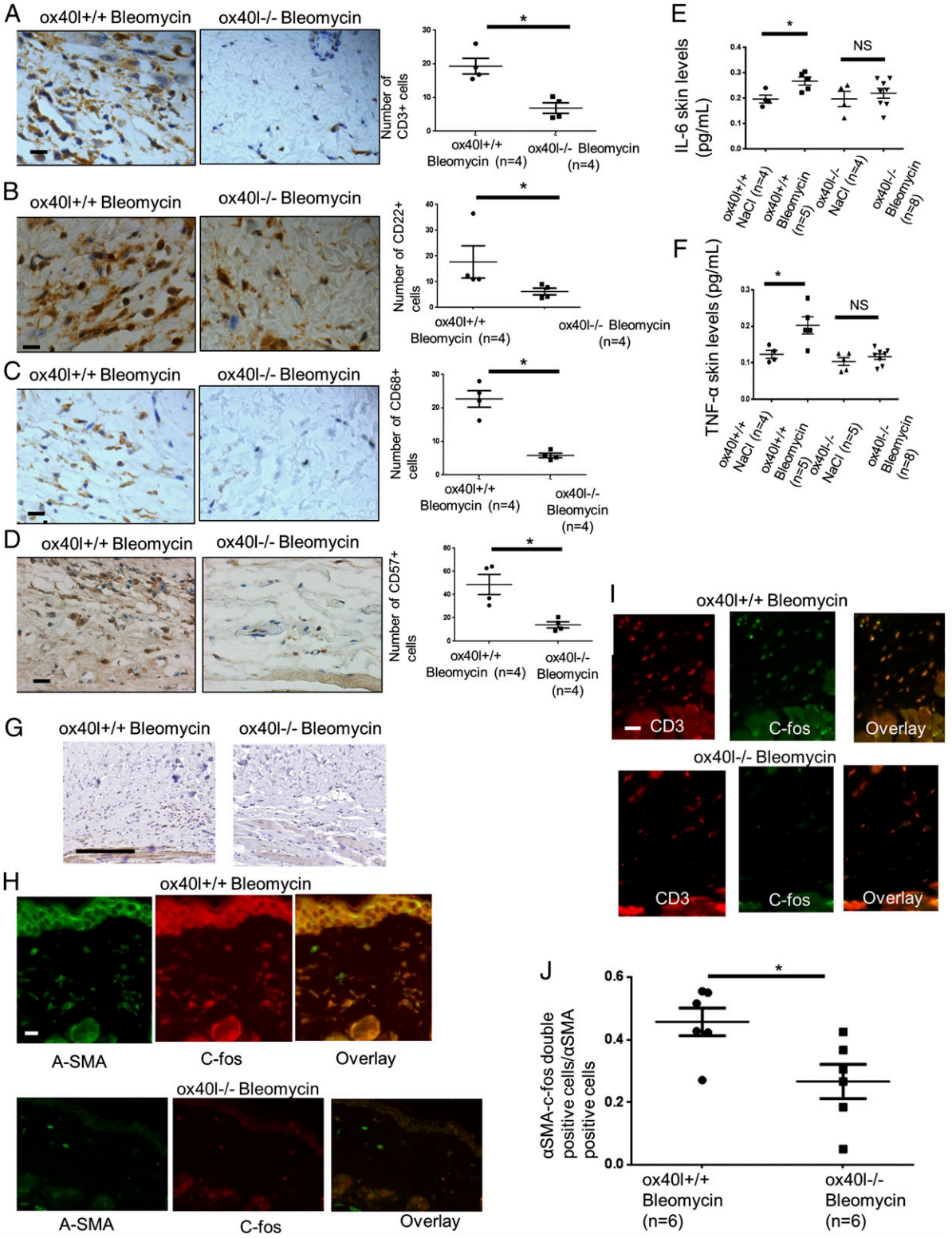

Fig. 4. Decrease in T cells, B cells, macrophages, NK cells, proinflammatory cytokines, and c-fos expression in lesional skin of OX40L-deficient mice subjected to bleomycin injections. (*A–D*) The number of $CD3^+$ T cells (*A*), $CD22^+$ B cells (*B*), $CD68^+$ macrophages (*C*), and NK cells (*D*) by immunohistochemistry in lesional skin of $ox40l^{+/+}$ and $ox40l^{-/-}$ mice challenged with bleomycin. Ten mice were used for these experiments. Representative sections stained by immunohistochemistry for CD3, CD22, CD68, and CD57 are shown. (Magnification: 400×.) (Scale bars: 10 μm.) (*E* and *F*) Skin levels of the cytokines Il-6 (*E*) and TNF-α (*F*) in $ox40l^{-/-}$ and $ox40l^{+/+}$ mice subjected to bleomycin. Sixteen mice were used for these experiments (four mice per group). All cytokine concentrations are normalized on total protein concentration. (*G*) Representative sections stained by immunohistochemistry for c-fos (magnification: 200×) from $ox40l^{+/+}$ and $ox40l^{-/-}$ mice receiving s.c. injections of bleomycin. The experiment was performed in two independent series of three mice. (Scale bar: 200 μm.) (*H*) c-Fos was expressed by $CD3^+$ T cells. The staining was performed in three independent series. (Magnification: 400×.) (Scale bar: 10 μm.) (*I*) c-Fos was expressed by α-SMA^+ cells. The staining was performed in three independent series. (Magnification: 400×.) (Scale bar: 10 μm.) (*J*) Semi-quantitative analysis of intensity of double staining among cells expressing α-SMA using ImageJ software. The staining was performed in six mice from each group (in two independent series). Values in *E*, *F*, and *J* are represented by dot blots with the mean ± SEM; $*P < 0.05$; two-tailed Mann–Whitney test. NS: nonsignificant.

Table 2. Interactive pathway analysis

Top canonical pathways	*P* value
Sulfite oxidation IV	1.49×10^{-2}
Androgen biosynthesis	1.80×10^{-2}
Inhibition of matrix metalloproteases	2.03×10^{-2}
L-DOPA degradation	2.96×10^{-2}
Thiosulfate disproportionation III	2.96×10^{-2}

A supervised analysis revealed the up-regulation of five pathways.

dermal fibrosis, ox40l$^{-/-}$ mice were lethally irradiated and reconstituted with bone marrow and spleen cells from ox40l$^{+/+}$ mice or ox40l$^{-/-}$ mice. One mouse died in the group reconstituted with cells from ox40l$^{+/+}$ mice. A trend was seen for increased thickness and collagen content of lesional skin in irradiated mice reconstituted with bone marrow and spleen cells from ox40L$^{+/+}$ mice as compared with mice reconstituted with cells from ox40l$^{-/-}$ mice (Fig. S4), but the trend did not reach significance. There was no significant difference between ox40l$^{-/-}$ mice reconstituted with bone marrow from ox40l$^{+/+}$ or ox40l$^{-/-}$ mice, suggesting that the blockage of OX40L acts on both hematopoietic cells and nonhematopoietic cells to prevent bleomycin-induced dermal fibrosis.

OX40L mAb Protects Against the Development of Bleomycin-Induced Fibrosis. For therapeutic purposes, we assessed the effect of a neutralizing mAb against murine OX40L in this model. Tolerance of the treatment was good. The anti-OX40L mAb significantly reduced dermal thickening by 31 ± 6% ($P = 0.002$), hydroxyproline content by 18 ± 5% ($P = 0.026$), and the number of myofibroblasts by 74 ± 67% ($P = 0.009$) (Fig. 5).

OX40L mAb Induces the Regression of Established Fibrosis in the Modified Bleomycin Model. Although the prevention of fibrosis is a major aim in the treatment of SSc, the clinical situation is most often characterized by patients who present with already established fibrosis. We addressed the antifibrotic effects of the anti-OX40L mAb in a model of established fibrosis. Treatment with the anti-OX40L mAb induced a regression of established fibrosis, with a decrease in dermal thickness by 26 ± 3% ($P = 0.002$), in collagen content by 22 ± 7% ($P = 0.020$), and in myofibroblasts recruitment by 42 ± 6% ($P = 0.027$) (Fig. 6).

OX40L mAb Does Not Protect Against Noninflammatory Skin Fibrosis in the Tight Skin 1 Mouse Model. Next, we aimed to determine whether OX40L inhibition was efficient in an inflammation-independent model of skin fibrosis, the tight skin 1 (Tsk-1) mouse model (12, 13). We did not observe any difference in hypodermal thickening and collagen content between Tsk-1 mice treated with the anti-OX40L mAb or with a control mAb (Fig. S5).

OX40L mAb Protects Against Fibrosing Alveolitis in the Fra-2 Transgenic Mouse Model. Because interstitial lung involvement and PAH are key prognostic factors in SSc (14), we aimed to assess the effects of the OX40L mAb in the Fra-2 mouse model, which exhibits these severe involvements (15, 16). Fra-2 transgenic mice displayed an increased expression of OX40 and OX40L in the skin and in the lungs as compared with control mice (Fig. S6). Treatment by anti-OX40L mAb was well tolerated. Micro-computed tomography (micro-CT) revealed higher lung density consistent with fibrosing alveolitis in Fra-2 mice treated with control mAb than in C57/BL6 mice ($P = 0.007$); this lung density was decreased significantly in Fra2 mice treated with the anti-OX40L mAb ($P = 0.004$). Restrictive lung disease was observed in Fra-2 mice treated with control mAb; these mice had a functional residual capacity equal to 44.7% of lung volume versus 77.4% in control mice ($P < 0.001$). Fra-2 mice receiving anti-OX40L mAb had a functional residual capacity of 71.4% of lung volume ($P < 0.001$). There was no significant difference at micro-CT between Fra-2 mice treated with anti-OX40L mAb and wild-type mice (Fig. 7). Fra-2 mice treated with control IgG were characterized by SSc-like features of nonspecific interstitial pneumonia at histology, with large patchy areas of lung parenchyma characterized by both diffuse cellular inflammation and collagen deposition (17). The lung fibrosis histological score was significantly higher in Fra-2 mice treated with control IgG than in Fra-2 mice receiving anti-OX40L mAb (mean score: 4.69 versus 2.69; $P = 0.032$) (Fig. 8 *A* and *B*). The lung fibrosis score was highly correlated with CT data (correlations with density score: ρ: 0.470, $P = 0.018$) and with forced residual capacity/lung volume (ρ: −0.846, 95% CI: −0.930–0.677; $P < 0.001$). Consistently, hydroxyproline content was reduced by 23 ± 9% ($P = 0.029$) (Fig. 8*C*). Second harmonic generation (SHG) microscopy showed a preferential perivascular distribution of fibrosis, suggesting fibrosing alveolitis (Fig. 8*D*). Scoring of fibrillar collagen deposits confirmed an increase in collagen scoring in Fra-2 mice receiving control IgG as compared Fra-2 mice treated with the anti-OX40L mAb ($P = 0.009$) (Fig. 8*E*).

OX40L mAb Protects Against PAH in the Fra-2 Transgenic Mouse Model. An increase in wall thickness and occlusion of pulmonary arteries, associated with massive perivascular inflammatory infiltrates, resembling SSc-associated PAH, were detected more frequently in Fra-2 mice treated with control antibody than in wild-type mice or Fra-2 mice receiving the anti-OX40L antibody (Fig. 9*A*). Obliterated vessels were undetectable in wild-type mice and in Fra-2 mice treated with anti-OX40L (0%) but were observed in 42.9% of Fra-2 mice receiving control antibody ($P = 0.02$). Completely muscularized or occluded vessels were observed in five of seven (71.4%) Fra-2 mice treated with control IgG and none of 10 wild-type and eight Fra-2 mice treated with anti-OX40L mAb ($P = 0.003$ and $P = 0.007$, respectively) (Fig. 9*B*). We did not observe coexpression of CD31 and α-SMA in the vessel walls of Fra-2 mice treated with control mAb, suggesting that PAH in this model was explained by the differentiation of resident fibroblasts into myofibroblasts rather than by endothelial-to-mesenchymal transition. This proliferation was decreased in Fra-2 mice treated with anti-OX40L antibody (Fig. 9*C*).

Discussion

Our study provides the first evidence, to our knowledge, that OX40L, a costimulatory molecule required for full activation of T cells, is implicated in the development of inflammation-driven skin, lung, and vessel fibrosis. SSc is the ideal disease for studying the events preceding the onset of fibrosis because the immune component and typical fibrotic events coincide in this condition. We identified increased OX40L expression in the lesional skin and serum of patients with SSc, particularly in patients with diffuse

Table 3. Gene set enrichment analysis

Top gene set enrichment analysis signaling pathways	Enrichment score	*P* value
PDGF receptor → AP-1/MYC	−0.51	$<1 \times 10^{-5}$
HGFR → AP-1/CREB/MYC	−0.50	$<1 \times 10^{-5}$
TGFBR → AP-1	−0.49	$<1 \times 10^{-5}$
Angiopoietin → AP-1	−0.47	$<1 \times 10^{-5}$
Notch → NFκB	−0.45	$<1 \times 10^{-5}$
IL1R → NFκB	−0.44	$<1 \times 10^{-5}$

A transcriptomic approach was performed to compare genes differentially expressed between ox40l$^{+/+}$ ($n = 3$) and ox40l$^{-/-}$ mice ($n = 4$) injected with bleomycin. Gene Set Enrichment Analysis showed an up-regulation of genes involved in two main pathways: the NFκB and AP1 pathways. CREB: cAMP response element binding protein; HGFR: hepatocyte growth factor receptor; PDGFR, PDGF receptor; TGFBR: TGF-β receptor.

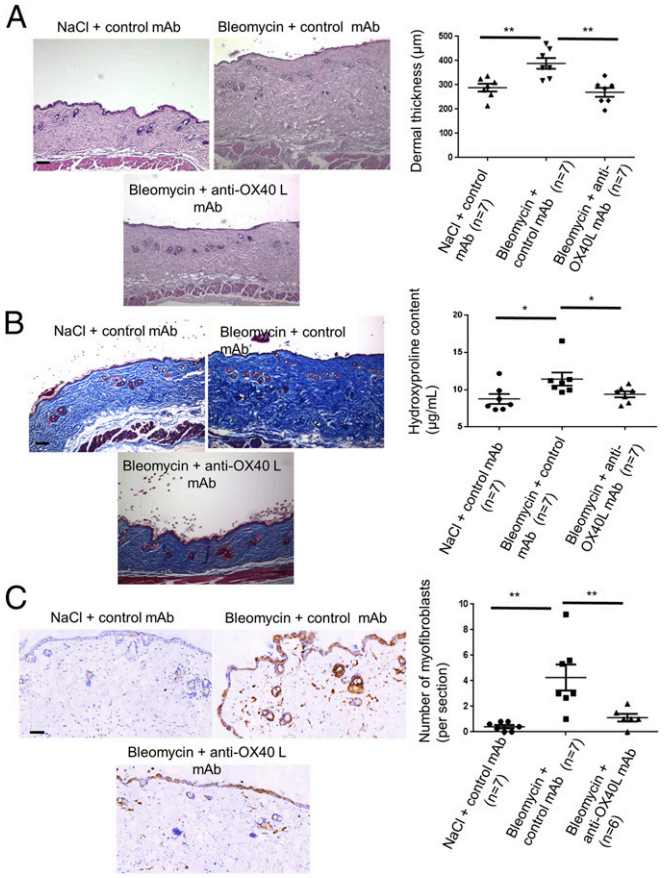

Fig. 5. Bleomycin-induced skin fibrosis is prevented upon OX40L inhibition with a neutralizing mAb. (*A*) Representative H&E-stained sections (magnification: 100×) from C57/Bl6 mice injected s.c. with NaCl and injected i.p. with IgG (control) ($n = 7$); C57/Bl6 mice injected s.c. with bleomycin injected i.p. with IgG (control) ($n = 7$); and C57/Bl6 mice injected s.c. with bleomycin and injected i.p. with anti-OX40L neutralizing mAb ($n = 7$). (Scale bar: 100 μm.) (*B*) Representative sections stained by trichrome. (Magnification: 100×.) (Scale bar: 100 μm.) The hydroxyproline assay evaluates collagen content. (*C*) Myofibroblasts were identified by positive staining for α-SMA in slides after counterstaining with hemalun. (Scale bar: 100 μm.) Values are represented by dot blots with mean ± SEM. The experiment was performed in two independent series. $*P < 0.05$; $**P < 0.01$; two-sided Mann–Whitney test.

cutaneous SSc. Diffuse SSc, defined by the highest extent of skin fibrosis, is associated with high morbidity and mortality (18). In addition to the expected expression of OX40L in perivascular T cells and B cells (4), we observed an expression, not previously reported, of OX40L by activated dermal fibroblasts, suggesting that mesenchymal cells can be directly activated by the OX40/OX40L pathway and thus promote collagen synthesis and fibrosis. Next, we showed that the inhibition of OX40L through complementary gene inactivation and targeted molecular strategies prevented and even induced the regression of bleomycin-induced dermal fibrosis. This widely used model mimics early and inflammatory stages of SSc. Blocking OX40L exerted antifibrotic effects in this model by decreasing the infiltration of T cells into lesional skin, as is consistent with previous reports in other preclinical models of autoimmune disorders (3, 19–22).

Our data support the notion that OX40L regulates the cytokine balance toward a proinflammatory and profibrotic profile, because lower levels of TNF-α and IL-6 were detected in ox40l$^{-/-}$ mice. This finding is consistent with the previous description of enhanced production of TNF-α and IL-6 through OX40/OX40L interaction (23). Reduced IL-6 release after OX40L invalidation also has been described in the murine model of encephalomyelitis (20). Herein, we confirmed that NF-κB is one of the central mediators of OX40L signaling (24). We also identified AP-1 as a downstream signaling pathway of OX40L. This finding has been scarcely reported to date but is consistent with the up-regulation of c-jun and c-fos mRNA observed in activated endothelial cells after binding OX40L (25). Interestingly, AP-1 is implicated both in inflammatory response and fibrosis. AP-1 is up-regulated in a TGF-β–dependent manner in SSc, and pharmacological inhibition of AP-1 prevents the pathological activation of dermal fibroblasts and the development of experimental dermal fibrosis (11). The reduced expression of c-jun and c-fos observed on T cells and fibroblasts from ox40l$^{-/-}$ mice upon bleomycin challenge suggests that OX40L may regulate inflammation and fibroblast activation through AP-1 signaling in inflammation-driven skin fibrosis. Despite its known predominant role in hematopoietic cells and the immune response, our results indicate that OX40L blocking does not act only through hematopoietic cells. Indeed, the results obtained in irradiated mice reconstituted with bone marrow and spleen cells from ox40l$^{+/+}$

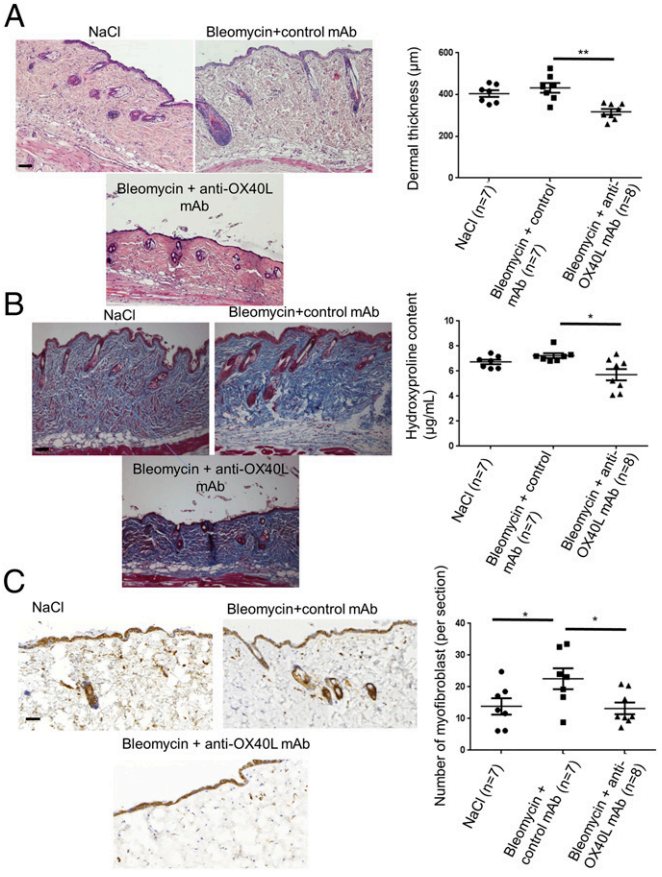

Fig. 6. Inhibition of OX40L with a neutralizing mAb induces regression of established fibrosis in the bleomycin mouse model. (*A*) Representative H&E-stained sections (magnification: 100×) from C57/Bl6 mice injected s.c. with bleomycin for 6 wk and injected i.p. with IgG (control) for the last 3 wk ($n = 7$); C57/Bl6 mice injected s.c. with bleomycin for 6 wk and injected i.p. in parallel with anti-OX40L neutralizing mAb for the last 3 wk ($n = 7$); and C57/Bl6 mice injected s.c. with bleomycin for 3 wk followed by s.c. injections of NaCl for the last 3 wk ($n = 8$). (Scale bar: 100 μm.) (*B*) Representative sections stained by trichrome. (Magnification: 100×.) (Scale bar: 100 μm.) The hydroxyproline assay evaluates collagen content. (*C*) Myofibroblasts were identified by positive staining for α-SMA in slides after counterstaining with hemalun. (Scale bar: 100 μm.) Twenty-two mice were used for these experiments. Results are represented by dot blots with mean ± SEM. The experiment was performed in two independent series. $*P < 0.05$; $**P < 0.01$; two-sided Mann–Whitney test.

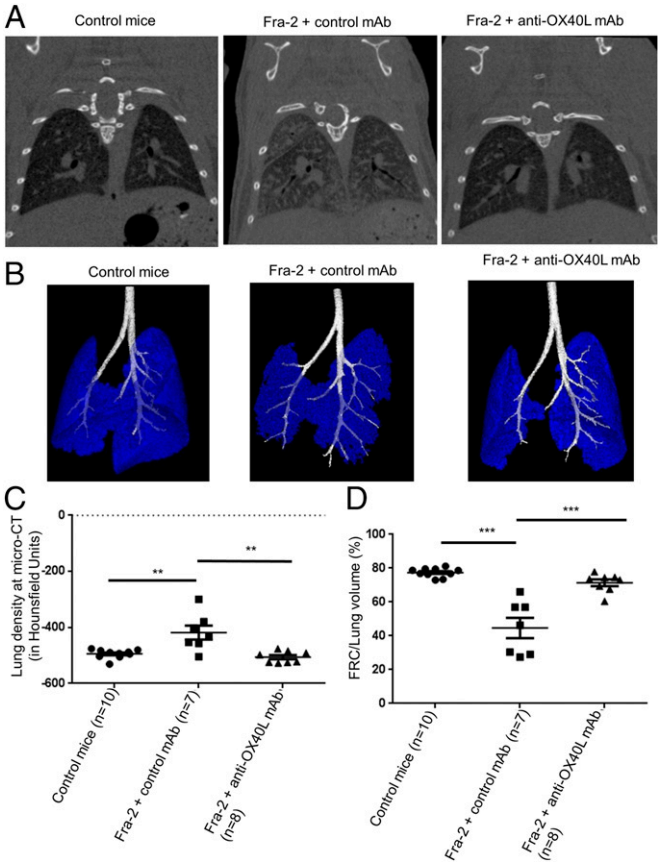

Fig. 7. Inhibition of OX40L prevents the development of fibrosing alveolitis: CT-scan data. (*A*) Fibrosing alveolitis was observed in Fra-2 mice receiving control IgG. Representative micro-CT images are shown. (*B*) Representative images of functional residual capacity (in blue) in different mice; bronchi are in white. (*C*) Increased lung density at micro-CT in Fra-2 transgenic mice treated with control IgG (n = 7) compared with Fra-2 mice treated with anti-OX40L mAb (n = 8) or C57/BL6 wild-type (control) mice (n = 10). (*D*) Residual lung volume, expressed as the percentage of functional residual capacity on total lung volume. Values are dot blots with the mean ± SEM; $^{**}P < 0.01$; $^{***}P < 0.001$; two-sided Mann–Whitney test.

mice and the in vitro data presented herein show that both hematopoietic and nonhematopoietic cells, including fibroblasts, are involved in the effects mediated by OX40L in the context of fibrosis.

Blocking OX40L with a specific mAb did not display antifibrotic properties in the Tsk-1 mouse model, which is characterized by endogenous activation of fibroblasts independent of inflammation; this result supports the proposition that the inflammatory environment is required for OX40L to exert profibrotic effects.

Our results highlight the substantial effects of blocking OX40L to prevent the severe organ damage characterizing SSc. Treatment with OX40L mAb markedly prevented fibrosing alveolitis in the Fra-2 transgenic mouse model by reducing inflammatory infiltrates, which are prominent features in this model. Consistently, OX40L transgenic mice spontaneous develop interstitial pneumonia accompanied by the significant production of anti-DNA antibody (26). This result is of particular importance because fibrosing alveolitis is the leading cause of death in SSc, and no efficient therapy is yet available to treat this devastating condition (14, 27). Furthermore, Fra-2 transgenic mice receiving anti-OX40L antibody had reduced perivascular inflammatory infiltrates and were protected against the vessel remodeling leading to PAH, the most extreme vascular phenotype of SSc (15, 16). The role of OX40L in PAH is also supported by the observations in OX40L transgenic mice, which spontaneously develop severe PAH associated with massive lymphocytic perivascular infiltration (28). Thus, OX40L inhibition may have the potential to address several aspects of SSc-PAH pathology that are not addressed by current therapies, which act mostly by relieving vasoconstriction. Fighting inflammation is a very appealing complementary strategy because both endothelial dysfunction and inflammation are intertwined with the initiation and progression of PAH.

In idiopathic PAH, proliferative vasculopathy results both from endothelial-to-mesenchymal transition and from the differentiation of resident fibroblasts into myofibroblasts. Our results suggest that the second mechanism is prominent in Fra-2 transgenic mice and that this proliferation was decreased in mice treated with anti-OX40L antibody.

Taken together, our results may have direct implications, because a human mAb, anti-OX40L, is available, and preliminary phase 2 data report that it was well tolerated in patients with

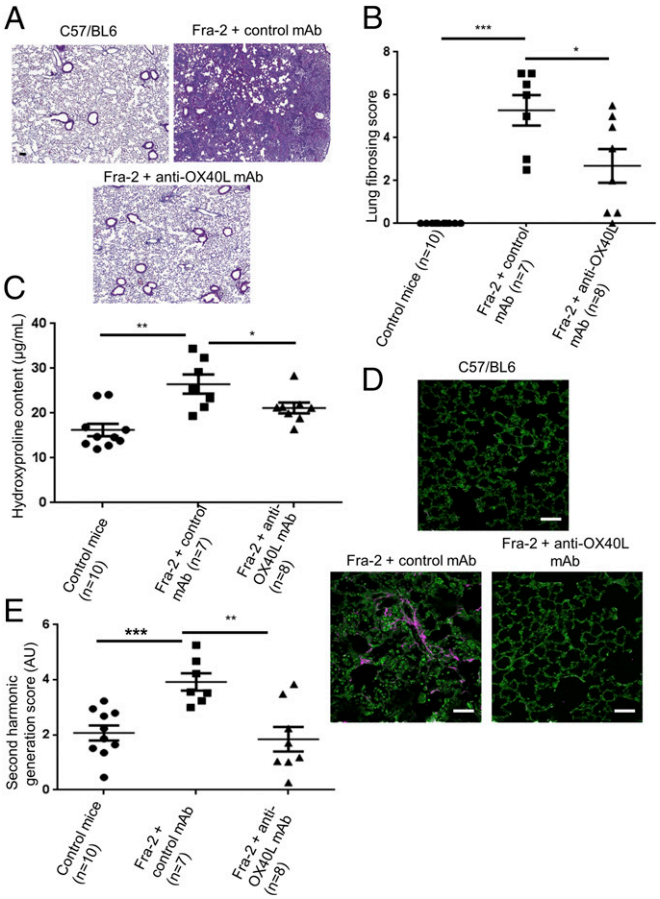

Fig. 8. Inhibition of OX40L prevents the development of fibrosing alveolitis: histological analysis. (*A*) Representative H&E-stained lung sections from Fra-2 mice treated with control IgG (n = 7), Fra-2 mice treated with anti-OX40L mAb (n = 8), and control C57/BL6 mice (n = 10). (Scale bar: 100 μm.) (*B*) Lung fibrosing score was significantly higher in Fra-2 mice receiving control mAb than in Fra-2 mice treated with anti-OX40L mAb. (*C*) The hydroxyproline assay evaluates collagen content. (*D*) SHG showed fibrillar collagen (in pink) in Fra-2 mice treated with control IgG. (Scale bar: 50 μm.) (*E*) Second harmonic scores were higher in Fra-2 mice receiving control IgG than in Fra-2 mice treated by anti-OX40L mAb or in control mice. Twenty-five mice were used for these experiments. Values in *B*, *C*, and *E* are represented by dot blots with means ± SEM. $^{*}P < 0.05$; $^{**}P < 0.01$; $^{***}P < 0.001$; two-sided Mann–Whitney test. AU: arbitrary units.

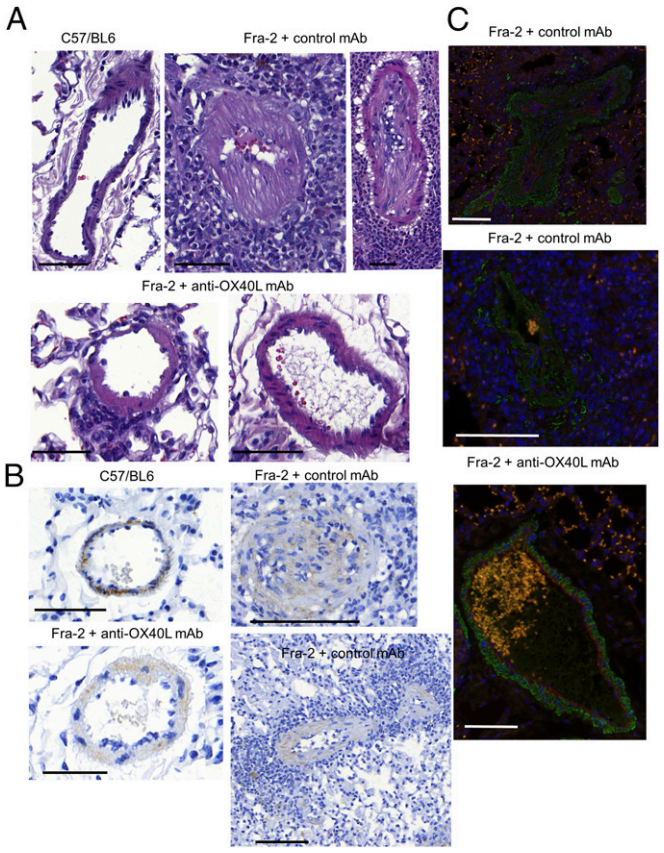

Fig. 9. Inhibition of OX40L prevents PAH in Fra-2 mice. (*A*) Representative H&E-stained sections from Fra-2 mice treated with control antibody (two representative pictures are shown: one vessel is almost occluded, and one is completely occluded), from C57/BL6 (control) mice, and from Fra-2 mice receiving anti-OX40L antibody (two representative pictures are shown: one vessel with a mild infiltrate, and one vessel without vasculopathy or inflammatory infiltrate). (Scale bars: 100 μm.) (*B*) Remodeling of the vessel was assessed by staining for α-SMA (immunohistochemistry) and was more pronounced in Fra-2 mice receiving control IgG (vessel occluded or almost completely occluded with a massive inflammatory infiltrate on two representative pictures) than in Fra-2 mice treated with anti-OX40L mAb or C57/BL6 (control) mice. Twenty-five mice were used for this experiment. (Scale bars: 100 μm.) (*C*) There was no costaining for CD31 (red) or α-SMA (green) in vessels from Fra-2 mice treated with control antibody or anti-OX40L antibody. Vasculopathy in Fra-2 mice receiving control antibody was related to the prominent proliferation of fibroblasts (marked by α-SMA) rather than endothelial-to-mesenchymal transition (no coexpression of CD31 and α-SMA). A massive perivascular infiltrate was noticed (DAPI). (Scale bars: 100 μm.)

mild allergic asthma (29). Fibrosis is the final common pathway hallmarking SSc and many other diseases. Therefore, blocking OX40L appears to be a promising strategy for SSc and for numerous fibrotic disorders. In addition, the anti-OX40L antibody offers the putative advantage of selectively targeting pathogenic T cells without causing generalized immunosuppression, possibly decreasing the risk of infections usually observed with other immunosuppressive drugs (3, 4, 10, 22, 30).

In addition to the lack of an effective therapy, another unmet clinical need in SSc and fibrotic disorders is the absence of reliable biomarkers predicting disease progression. Soluble OX40L appears to be a promising biomarker, because increased serum levels were detected in SSc patients with severe skin or lung disease at baseline, and, of particular interest, high concentrations also were predictive of worsening skin and lung fibrosis during the follow-up period. The data regarding lung fibrosis that were independently replicated in a well-structured cohort support the robustness of OX40L as a prognostic marker for this severe complication, which is the leading cause of death in SSc.

Materials and Methods

Patients and Skin Biopsies. OX40L was quantified by ELISA in the serum of 177 patients with SSc and 100 healthy age- and sex-matched volunteers using the Human Soluble OX40L (sOX40L) ELISA kit (Cusabio). The replication study cohort was derived from the prospective, observational Oslo University Hospital SSc cohort study dedicated to lung fibrosis assessment (31).

Paraffin-embedded sections of lesional skin biopsies were obtained from eight patients with SSc (three patients with limited SSc and five patients with diffuse cutaneous forms) and from five healthy age- and sex-matched healthy volunteers.

Fibroblast Cultures. Fibroblast cultures were obtained from biopsies of involved skin of patients with SSc and skin of healthy volunteers. Mouse fibroblasts cultures were obtained from samples taken from the ears of mice. Fibroblasts were prepared by outgrowth cultures. Fibroblasts from passages 2–3 were used for the experiments.

Bleomycin-Induced Dermal Fibrosis in OX40L-Deficient Mice. Skin fibrosis was induced in 6-wk-old male mice by local injections of bleomycin for 3 wk (32). Injections (s.c.) of NaCl were used as controls. The four groups consisted of 30 mice in total. Validated parameters (11, 33) were used for evaluation. Mice were killed by cervical dislocation after 3 wk of treatment, and the injected skin was processed further for analysis.

Irradiation and Graft. In all, 20 5- to 7-wk-old ox40l$^{-/-}$ mice (10 females and 10 males) were included. Recipient mice were lethally irradiated and reconstituted with spleen and bone marrow cells from ox40l$^{+/+}$ mice ($n = 7$) or from ox40l$^{+/+}$ mice ($n = 7$), as previously described (34). Seven ox40l$^{-/-}$ mice were not irradiated and were used as controls. Beginning on the day after irradiation, mice were injected s.c. with bleomycin for 3 wk, as previously described.

Prevention and Treatment of Bleomycin-Induced Fibrosis with anti-OX40L mAb. In the preventive protocol, one group of seven mice received i.p. injections of 300 μg anti-OX40L mAb (RM134L, rat IgG2b) in 100 μL PBS three times/wk over a 3-wk period starting on the day before the first injection of bleomycin. Two control groups of seven mice were treated with an equivalent amount of control rat IgG (Sigma) and were injected with bleomycin and NaCl, respectively. The three groups consisted of 21 mice in total. In the therapeutic protocol we assessed the effects of OX40L inhibition in established dermal fibrosis. Two groups of mice were challenged with bleomycin for 6 wk and were treated in parallel with i.p. injection of 300 μg anti-OX40L mAb or control IgG three times/wk, beginning after the third week of bleomycin. The third group received bleomycin injections for 3 wk followed by NaCl injections for the next 3 wk to control for the spontaneous regression of fibrosis. Mice were killed by cervical dislocation after 6 wk of treatment.

Evaluation of Dermal Thickness. Dermal thickness was analyzed at 100× magnification by measuring the distance between the epidermal–dermal junction and the dermal–s.c. fat junction at four sites on H&E-stained skin sections. Measurements were made by two independent blinded examiners (M.F. and M.E.), as previously described (33, 35).

Collagen Measurements. The collagen content in lesional skin samples was explored by hydroxyproline assay, as previously described (33, 35). For direct visualization of collagen fibers, trichrome staining was performed using the Masson's Trichrome Staining Kit (Sigma-Aldrich).

Immunohistochemistry for α-SMA, OX40L, c-Fos, c-Jun, CD3, CD22, CD57, and CD68. Myofibroblasts were identified by staining for α-SMA as previously described (33). T cells, B cells, NK cells, macrophages, and c-fos^{+} and c-jun^{+} cells were identified by staining for CD3, CD22, CD57, CD68, c-fos, and c-jun, respectively (all antibodies were from Abcam) (33, 35).

The expression of OX40L in lesional skin from patients with SSc and in skin from controls was detected by staining with polyclonal rabbit anti-human OX40L antibody or isotype control (Sigma-Aldrich). The intensity of OX40L immunostaining was quantified with ImageJ software.

Immunofluorescence for OX40L, CD3, CD22, CD31, α-SMA, c-Fos, and CD90. For costaining experiments, immunofluorescent staining was performed in lesional skin from patients with SSc. Fibroblasts were identified by staining for

CD90 (Abcam). The intensity of α-SMA$^+$ cells expressing c-fos was quantified with ImageJ software.

Inflammatory Cytokine Measurement in Lesional Skin Samples of Bleomycin-Treated Mice. Cytokine levels were measured in the skin of 16 ox40l$^{-/-}$ and ox40l$^{+/+}$ mice subjected to bleomycin or NaCl injections (four mice per group), as previously described (33, 35). Protein concentration was determined with the amidoblack method (36). Skin lysates were assayed for TNF-α, IL-6, IFN-γ, IL-4, IL-10, and IL-17.

Effects of OX40L Inhibition in the Tsk-1 Mouse Model. Starting at 5 wk of age, five Tsk-1 mice were treated with 300 μg anti-OX40L mAb and four Tsk-1 mice were treated with control IgG. A third group consisted of five control mice homozygous for the pallid spontaneous mutation (pa/pa mice). Mice were killed by cervical dislocation at the age of 10 wk to analyze the hypodermal thickness and the hydroxyproline content in lesional skin.

Transcriptomic Approach. Skin samples from three ox40l$^{+/+}$ and four ox40l$^{-/-}$ mice treated with bleomycin were defrosted, extracted, and hybridized at the same time. Affymetrix microarray technology was used to analyze gene expression levels.

Extraction protocol. Total RNA were extracted from lesional skin samples of three ox40l$^{+/+}$ and four ox40l$^{-/-}$ mice treated with bleomycin using the RNeasy Mini Kit with DNase I digestion according to the manufacturer's instructions.

Transcriptomes preparation and data analysis. Samples were prepared according to standard practices of the GENOM'IC facility of the Institut Cochin. All microarray data and information have been submitted to the National Center for Biotechnology Information Gene Expression Omnibus site (accession no. GSE73705). Data were robust multiarray normalized with Bioconductor. We first controlled and analyzed data in an unsupervised way by principal components analysis and used ANOVA to extract differentially expressed genes with the Partek Genomics Suite. Enrichment analysis was carried out using Interactive Pathway Analysis and Pathway Studio.

Prevention of Fibrosing Alveolitis and PAH in the Fra-2 Model. Two groups of Fra-2 transgenic mice were treated by anti-OX40L mAb ($n = 8$ mice) or control rat IgG (n = 7 mice) beginning on week 13 of development. Two control groups of five C57/BL6 mice were treated with anti-OX40L mAb or control rat IgG, respectively. Mice were killed by cervical dislocation at age 17 wk.

Assessment of Fibrosing Alveolitis by Micro-CT. Fibrosing alveolitis was evaluated using micro-CT 2 d before mice were killed. Means of lung density of both groups were determined by evaluating all CT scans acquired from the apices to the bases of the lungs. Furthermore, the volume of functional lung parenchyma corresponding to functional residual capacity (FRC) was drawn manually, excluding fibrotic area and vessels. Percentages of FRC on total lung volumes were calculated. The CT expert (J.S.) was blinded to the background of mice, to the treatment, and to the results of the histological assessment.

Histopathologic Assessment of Fibrosing Alveolitis. Lung sections were stained with H&E. The severity of fibrosing alveolitis was semiquantitatively assessed on a scale of 0–8 according to the method described by Ashcroft et al. (37) by two examiners (O.A. and M.E.) blinded to the genotype and the treatment. Hydroxyproline content in lung biopsies was assessed as previously described.

Nonlinear Microscopy and SHG Processing. A multiphoton inverted-stand Leica SP5 microscope (Leica Microsystems GmbH) was used for tissue imaging. Two fixed thresholds were chosen to distinguish biological material from the background signal [two-photon excited harmonic (TPEF) images] and specific collagen fibers (SHG images). The SHG score was established by comparing the area occupied by the collagen relative to the sample surface. Image processing and analysis (thresholding and SHG scoring) were performed using ImageJ homemade routines (imagej.nih.gov/ij) as previously described (38). Results were normalized to control C57/BL6 mice.

Vessel Remodeling. In each mouse, a total of 15 vessels and their accompanying alveolar ducts or alveoli were examined by two observers (O.A. and M.E.) masked to the genotype and treatment. Each vessel was categorized as nonmuscular (no evidence of vessel wall muscularization), partially or completely muscular (smooth muscle cells identifiable in part or in the entire vessel circumference), or occluded. Muscularization was defined as the presence of typical smooth muscle cells stained with α-SMA. All images were taken with a Lamina multilabel slide scanner.

Statistics. All data analyses were performed using GraphPad. Data are presented as mean (SEM) for continuous variables and as numbers (percentages) for categorical variables. Data were analyzed statistically using Fischer tests for differences in frequency and the Mann–Whitney test for comparisons between two continuous variables. A P value of less than 0.05 was considered statistically significant. Further details regarding materials and methods are provided in *SI Materials and Methods*.

Study Approval. All patients and controls signed a consent form approved by the local institutional review boards [CPP (Comité de Protection des Personnes) Paris Ile de France 3]. The local ethical committee [CEEA (comité d'éthique en experimentation animale) 34 of Paris Descartes University] approved all animal experiments [agreements no. CEEA34.JA.023.12 and no. 15-031 (Apafis 2015080901097845 and 2015062619109294)].

ACKNOWLEDGMENTS. We thank the following individuals for excellent technical assistance: Avigail Bismuth, Lucille Desallais, Florence Morin, Maryline Favier, and Corinne Lesaffre (Histology Facility of the Cochin Institute); B. Durel (Cochin Imaging Facility); M. Andrieu [Immunology Flow Cytometry Facility (CyBio Platform) of the Cochin Institute]; F. Letourneur and F. Dumont (Genomics Platform of the Cochin Institute); and Prof. Catherine Chaussain (Dental School of the Paris Descartes University, EA 2496). This work was supported by INSERM, ATIP/AVENIR programme, Société Française de Rhumatologie, Fondation pour la Recherche Médicale, the Arthritis Foundation, the Institut Servier, and Japan Society for the Promotion of Science Grant-in-Aid for Scientific Research 26293087.

1. Friedman SL, Sheppard D, Duffield JS, Violette S (2013) Therapy for fibrotic diseases: Nearing the starting line. *Sci Transl Med* 5(167):167sr1.
2. Varga J, Pasche B (2009) Transforming growth factor beta as a therapeutic target in systemic sclerosis. *Nat Rev Rheumatol* 5(4):200–206.
3. Sugamura K, Ishii N, Weinberg AD (2004) Therapeutic targeting of the effector T-cell co-stimulatory molecule OX40. *Nat Rev Immunol* 4(6):420–431.
4. Ishii N, Takahashi T, Soroosh P, Sugamura K (2010) OX40-OX40 ligand interaction in T-cell-mediated immunity and immunopathology. *Adv Immunol* 105:63–98.
5. Webb GJ, Hirschfield GM, Lane PJL (2016) OX40, OX40L and autoimmunity: A comprehensive review. *Clin Rev Allergy Immunol* 50(3):312–332.
6. Gourh P, et al. (2010) Association of TNFSF4 (OX40L) polymorphisms with susceptibility to systemic sclerosis. *Ann Rheum Dis* 69(3):550–555.
7. Bossini-Castillo L, et al. (2011) A replication study confirms the association of TNFSF4 (OX40L) polymorphisms with systemic sclerosis in a large European cohort. *Ann Rheum Dis* 70(4):638–641.
8. Coustet B, et al. (2012) Independent replication and meta analysis of association studies establish TNFSF4 as a susceptibility gene preferentially associated with the subset of anticentromere-positive patients with systemic sclerosis. *J Rheumatol* 39(5):997–1003.
9. Komura K, et al. (2008) Increased serum soluble OX40 in patients with systemic sclerosis. *J Rheumatol* 35(12):2359–2362.
10. Gwyer Findlay E, et al. (2014) OX40L blockade is therapeutic in arthritis, despite promoting osteoclastogenesis. *Proc Natl Acad Sci USA* 111(6):2289–2294.
11. Avouac J, et al. (2012) Inhibition of activator protein 1 signaling abrogates transforming growth factor β-mediated activation of fibroblasts and prevents experimental fibrosis. *Arthritis Rheum* 64(5):1642–1652.
12. Beyer C, Schett G, Distler O, Distler JHW (2010) Animal models of systemic sclerosis: Prospects and limitations. *Arthritis Rheum* 62(10):2831–2844.
13. Green MC, Sweet HO, Bunker LE (1976) Tight-skin, a new mutation of the mouse causing excessive growth of connective tissue and skeleton. *Am J Pathol* 82(3):493–512.
14. Tyndall AJ, et al. (2010) Causes and risk factors for death in systemic sclerosis: A study from the EULAR Scleroderma Trials and Research (EUSTAR) database. *Ann Rheum Dis* 69(10):1809–1815.
15. Maurer B, et al. (2012) Fra-2 transgenic mice as a novel model of pulmonary hypertension associated with systemic sclerosis. *Ann Rheum Dis* 71(8):1382–1387.
16. Maurer B, et al. (2009) Transcription factor fos-related antigen-2 induces progressive peripheral vasculopathy in mice closely resembling human systemic sclerosis. *Circulation* 120(23):2367–2376.
17. du Bois RM (2007) Mechanisms of scleroderma-induced lung disease. *Proc Am Thorac Soc* 4(5):434–438.
18. Frech TM, et al. (2013) Treatment of early diffuse systemic sclerosis skin disease. *Clin Exp Rheumatol* 31(2, Suppl 76):166–171.
19. Higgins LM, et al. (1999) Regulation of T cell activation in vitro and in vivo by targeting the OX40-OX40 ligand interaction: Amelioration of ongoing inflammatory bowel disease with an OX40-IgG fusion protein, but not with an OX40 ligand-IgG fusion protein. *J Immunol* 162(1):486–493.
20. Ndhlovu LC, Ishii N, Murata K, Sato T, Sugamura K (2001) Critical involvement of OX40 ligand signals in the T cell priming events during experimental autoimmune encephalomyelitis. *J Immunol* 167(5):2991–2999.
21. Carboni S, et al. (2003) CD134 plays a crucial role in the pathogenesis of EAE and is upregulated in the CNS of patients with multiple sclerosis. *J Neuroimmunol* 145(1-2):1–11.

22. Croft M, So T, Duan W, Soroosh P (2009) The significance of OX40 and OX40L to T-cell biology and immune disease. *Immunol Rev* 229(1):173–191.
23. Ohshima Y, et al. (1997) Expression and function of OX40 ligand on human dendritic cells. *J Immunol* 159(8):3838–3848.
24. Song J, So T, Croft M (2008) Activation of NF-kappaB1 by OX40 contributes to antigen-driven T cell expansion and survival. *J Immunol* 180(11):7240–7248.
25. Matsumura Y, Hori T, Kawamata S, Imura A, Uchiyama T (1999) Intracellular signaling of gp34, the OX40 ligand: Induction of c-jun and c-fos mRNA expression through gp34 upon binding of its receptor, OX40. *J Immunol* 163(6):3007–3011.
26. Murata K, et al. (2002) Constitutive OX40/OX40 ligand interaction induces autoimmune-like diseases. *J Immunol* 169(8):4628–4636.
27. Bagnato G, Harari S (2015) Cellular interactions in the pathogenesis of interstitial lung diseases. *Eur Respir Rev* 24(135):102–114.
28. Rabieyousefi M, et al. (2011) Indispensable roles of OX40L-derived signal and epistatic genetic effect in immune-mediated pathogenesis of spontaneous pulmonary hypertension. *BMC Immunol* 12:67.
29. Gauvreau GM, et al. (2014) OX40L blockade and allergen-induced airway responses in subjects with mild asthma. *Clin Exp Allergy* 44(1):29–37.
30. Humphreys IR, et al. (2003) A critical role for OX40 in T cell-mediated immunopathology during lung viral infection. *J Exp Med* 198(8):1237–1242.
31. Hoffmann-Vold A-M, et al. (2015) Predictive value of serial high-resolution computed tomography analyses and concurrent lung function tests in systemic sclerosis. *Arthritis Rheumatol* 67(8):2205–2212.
32. Yamamoto T (2010) Animal model of systemic sclerosis. *J Dermatol* 37(1):26–41.
33. Avouac J, et al. (2013) Critical role of the adhesion receptor DNAX accessory molecule-1 (DNAM-1) in the development of inflammation-driven dermal fibrosis in a mouse model of systemic sclerosis. *Ann Rheum Dis* 72(6):1089–1098.
34. Kavian N, et al. (2012) Sunitinib inhibits the phosphorylation of platelet-derived growth factor receptor β in the skin of mice with scleroderma-like features and prevents the development of the disease. *Arthritis Rheum* 64(6):1990–2000.
35. Avouac J, et al. (2011) Inactivation of the transcription factor STAT-4 prevents inflammation-driven fibrosis in animal models of systemic sclerosis. *Arthritis Rheum* 63(3):800–809.
36. Kamel H, et al. (1978) Comparison of gold levels and distribution in guinea pig serum. *Arthritis Rheum* 21(4):441–446.
37. Ashcroft T, Simpson JM, Timbrell V (1988) Simple method of estimating severity of pulmonary fibrosis on a numerical scale. *J Clin Pathol* 41(4):467–470.
38. Gailhouste L, et al. (2010) Fibrillar collagen scoring by second harmonic microscopy: A new tool in the assessment of liver fibrosis. *J Hepatol* 52(3):398–406.
39. Subcommittee for scleroderma criteria of the American Rheumatism Association Diagnostic and Therapeutic Criteria Committee (1980) Preliminary criteria for the classification of systemic sclerosis (scleroderma). *Arthritis Rheum* 23(5):581–590.
40. LeRoy EC, et al. (1988) Scleroderma (systemic sclerosis): Classification, subsets and pathogenesis. *J Rheumatol* 15(2):202–205.
41. Humbert M, McLaughlin VV (2009) The 4th world symposium on pulmonary hypertension. *J Am Coll Cardiol* 54(1 Suppl):S1–117.
42. Clements PJ, et al. (1993) Skin thickness score in systemic sclerosis: An assessment of interobserver variability in 3 independent studies. *J Rheumatol* 20(11):1892–1896.
43. Hoffmann-Vold A-M, Gunnarsson R, Garen T, Midtvedt Ø, Molberg Ø (2015) Performance of the 2013 American College of Rheumatology/European League Against Rheumatism Classification Criteria for Systemic Sclerosis (SSc) in large, well-defined cohorts of SSc and mixed connective tissue disease. *J Rheumatol* 42(1):60–63.
44. Goh NSL, et al. (2008) Interstitial lung disease in systemic sclerosis: A simple staging system. *Am J Respir Crit Care Med* 177(11):1248–1254.